



# Maf promotes osteoblast differentiation in mice by mediating the age-related switch in mesenchymal cell differentiation

Keizo Nishikawa,<sup>1,2</sup> Tomoki Nakashima,<sup>1,2,3</sup> Shu Takeda,<sup>4</sup> Masashi Isogai,<sup>5</sup> Michito Hamada,<sup>5</sup> Ayako Kimura,<sup>4</sup> Tatsuhiko Kodama,<sup>6</sup> Akira Yamaguchi,<sup>7</sup> Michael J. Owen,<sup>8</sup> Satoru Takahashi,<sup>5</sup> and Hiroshi Takayanagi<sup>1,2,3</sup>

<sup>1</sup>Department of Cell Signaling, Graduate School of Medical and Dental Sciences, Tokyo Medical and Dental University, Tokyo, Japan.

<sup>2</sup>Global Center of Excellence Program, International Research Center for Molecular Science in Tooth and Bone Diseases, and

<sup>3</sup>Japan Science and Technology Agency, ERATO, Takayanagi Osteonetwork Project, Tokyo, Japan. <sup>4</sup>Department of Orthopaedic Surgery, Graduate School of Medical and Dental Sciences, Tokyo Medical and Dental University, Tokyo, Japan. <sup>5</sup>Institute of Basic Medical Sciences and Laboratory Animal Resource Center, University of Tsukuba, Tsukuba, Japan. <sup>6</sup>Department of Molecular Biology and Medicine, Research Center for Advanced Science and Technology, University of Tokyo, Tokyo, Japan. <sup>7</sup>Department of Oral Pathology, Graduate School of Medical and Dental Sciences, Tokyo Medical and Dental University, Tokyo, Japan.

<sup>8</sup>GlaxoSmithKline, Stevenage, United Kingdom.

**Aging leads to the disruption of the homeostatic balance of multiple biological systems. In bone marrow multipotent mesenchymal cells undergo differentiation into various anchorage-dependent cell types, including osteoblasts and adipocytes. With age as well as with treatment of antidiabetic drugs such as thiazolidinediones, mesenchymal cells favor differentiation into adipocytes, resulting in an increased number of adipocytes and a decreased number of osteoblasts, causing osteoporosis. The mechanism behind this differentiation switch is unknown. Here we show an age-related decrease in the expression of *Maf* in mouse mesenchymal cells, which regulated mesenchymal cell bifurcation into osteoblasts and adipocytes by cooperating with the osteogenic transcription factor *Runx2* and inhibiting the expression of the adipogenic transcription factor *Pparg*. The crucial role of *Maf* in both osteogenesis and adipogenesis was underscored by *in vivo* observations of delayed bone formation in perinatal *Maf*<sup>-/-</sup> mice and an accelerated formation of fatty marrow associated with bone loss in aged *Maf*<sup>+/-</sup> mice. This study identifies a transcriptional mechanism for an age-related switch in cell fate determination and may provide a molecular basis for novel therapeutic strategies against age-related bone diseases.**

## Introduction

A progressive and irreversible accumulation of DNA damage, which is triggered by telomere shortening and various stressors such as oxidative stress, contributes to cellular senescence and organismal aging (1, 2), but how aging is related to the disruption of the homeostatic balance of cell differentiation from a common progenitor is not well understood. Bone marrow contains multipotent mesenchymal progenitor cells, which differentiate into various anchorage-dependent cell types, including adipocytes and osteoblasts (3, 4). With age, mesenchymal cells in the bone marrow become inclined to undergo differentiation into adipocytes rather than osteoblasts (5–7), resulting in an increased number of adipocytes and a decreased number of osteoblasts, causing osteoporosis. Adipocytes are also known to directly inhibit functions of other cells in the bone marrow, including hematopoietic stem cells and osteoblasts (8–11). Since an increase in marrow fat along with bone loss is observed in diabetic patients treated with thiazolidinediones (TZDs) (12), understanding the mechanism of this differentiation switch has substantial relevance to both the management of age-related osteoporosis and secondary osteoporosis after such drug treatment. However, the change in mesenchymal cell differentiation cannot be adequately explained by cellular

senescence or the cell cycle arrest caused by DNA damage. While estrogen deficiency causes postmenopausal osteoporosis (6, 13), it has been suggested that the downregulation of cytokines and hormones, such as IGF1, TGFβ1, IL-11, and growth hormone, is correlated with age-related bone loss (6, 14, 15). However, a cell-intrinsic mechanism that regulates the age-related switch in mesenchymal cell differentiation remains to be elucidated. Here we report an age-related decrease in the expression of *Maf* in mesenchymal cells and present evidence that *Maf* regulates mesenchymal cell bifurcation into osteoblasts and adipocytes. This study establishes the crucial role of the *Maf*-mediated transcriptional program in the physiological and age-related regulation of mesenchymal cell lineage, which may facilitate the development of new therapeutic strategies against bone and metabolic diseases.

## Results

*A genome-wide screening of transcription factors involved in the age-related decrease in bone formation.* To identify the transcription factors involved in age-related bone loss, we performed a genome-wide screening of mRNAs expressed in cells derived from mouse calvaria during osteoblastogenesis. Among 1,470 transcription factors, we identified 163 genes related to osteogenic function; the identifying characteristic of these factors was that their expression was increased by more than 4-fold during osteoblastogenesis (Figure 1A and Supplemental Table 1, A and B; supplemental material

**Conflict of interest:** The authors have declared that no conflict of interest exists.

**Citation for this article:** *J Clin Invest.* 2010;120(10):3455–3465. doi:10.1172/JCI42528.

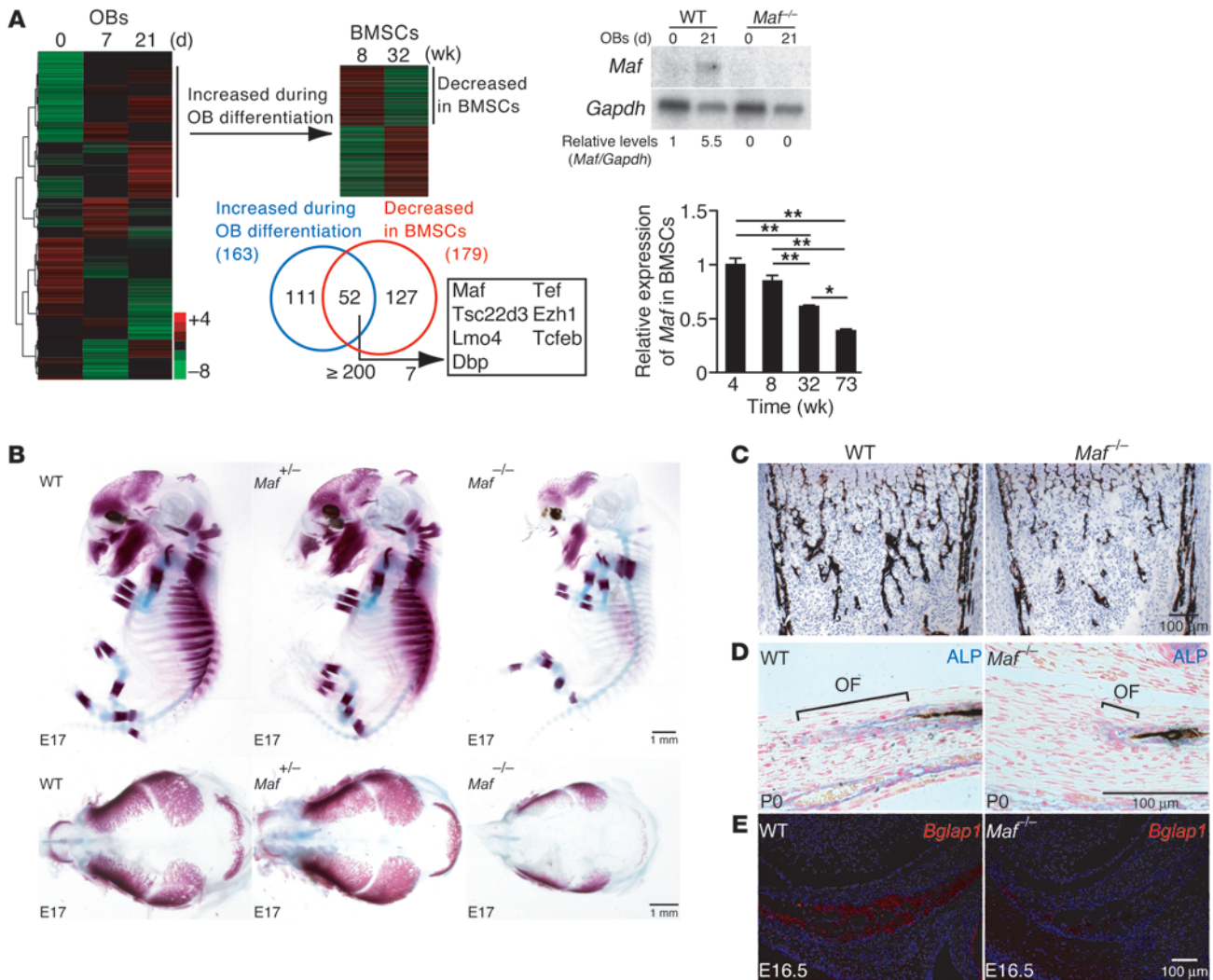


**Figure 1** Impaired bone formation in *Maf*<sup>-/-</sup> mice. **(A)** A genome-wide screening of transcription factor mRNAs during in vitro differentiation of osteoblasts (OBs) and a comparison of their expression between 8- and 32-week-old BMSCs. The increase in *Maf* expression during osteoblastogenesis was confirmed in calvarial osteoblasts (RNA blot analysis, right top). *Maf* expression was markedly lower in BMSCs derived from the aged mice (real-time RT-PCR analysis, right bottom). Screening results are summarized in the Venn diagram. \**P* < 0.05; \*\**P* < 0.01. **(B)** Alizarin red/alcian blue staining of E17 embryos (top). Top view of calvaria (bottom). Images in **B** are composites. **(C)** Histology (von Kossa staining) and micro-computed tomography analysis of WT and *Maf*<sup>-/-</sup> littermates at P0 (*n* = 3). Scale bar: 100 μm. **(D)** ALP and von Kossa staining of osteogenic fronts (OFs) in the calvaria of WT and *Maf*<sup>-/-</sup> littermates. Scale bar: 100 μm. **(E)** Expression of *Bglap1* in the calvaria of WT and *Maf*<sup>-/-</sup> mice (in situ hybridization). Scale bar: 100 μm.

available online with this article; doi:10.1172/JCI42528DS1). To identify age-related genes, we also comprehensively analyzed the mRNAs expressed by bone marrow stromal cells (BMSCs) derived from 8- and 32-week-old mice, which resulted in identifications of 179 genes, the expression of which was decreased in the aged mice by more than 2 fold (Supplemental Table 1C). Fifty-two genes met both criteria (Supplemental Table 1D), from which we selected 7 genes preferentially expressed in BMSCs (with an average difference greater than 200). Among these 7 genes, we identified *Maf* (also known as c-Maf) to be the most highly expressed in the BMSCs. We confirmed that the expression of *Maf* increased during osteoblastogenesis, using calvarial and BMSCs (Figure 1A, right top, and Supplemental Figure 1A), and decreased with age (Figure 1A, right bottom, and Supplemental Figure 1B). *Maf*, a

basic leucine zipper transcription factor, is known to be involved in the regulation of diverse developmental processes such as lens fiber elongation (16) and Th2 cell differentiation (17, 18). Although it has been documented that transcription factors such as  $\Delta$ Fosb, Taz, Esr1, Msx2, and Cebpb $\beta$  regulate the bifurcation of osteoblast/adipocyte differentiation (7, 19, 20), the expression of  $\Delta$ Fosb was increased in aged BMSCs (Supplemental Figure 2) and the other 4 factors were not included in the 179 age-related genes (Supplemental Table 1C). These results suggest that *Maf* is one of the potential candidate genes underlying an age-related decrease in osteoblastogenesis.

*The indispensable role of Maf in osteogenesis.* Since *Maf*<sup>-/-</sup> mice usually die immediately after birth (16), we investigated the role of *Maf* in osteogenesis by analyzing the skeletal development of perinatal



**Table 1**  
Skeletal development of perinatal *Maf*<sup>-/-</sup> mice

	WT	<i>Maf</i> <sup>-/-</sup>
BV/TV (%)	29.51 ± 0.15	23.56 ± 0.32 <sup>A</sup>
Tb.N (mm <sup>-1</sup> )	13.43 ± 0.26	11.81 ± 0.33 <sup>B</sup>
Tb.Sp (μm)	51.86 ± 1.59	64.98 ± 1.46 <sup>A</sup>
Tb.Th (μm)	22.47 ± 0.03	20.36 ± 0.63 <sup>B</sup>

Microcomputed tomography analysis of WT and *Maf*<sup>-/-</sup> littermates at P0. BV/TV, bone volume/tissue volume, Tb.N, trabecular number, Tb.Sp, trabecular separation, and Tb.Th, trabecular thickness. <sup>A</sup>*P* < 0.01. <sup>B</sup>*P* < 0.05.

*Maf*<sup>-/-</sup> mice. Bone formation was severely impaired in both the long and calvarial bones in the embryos of *Maf*<sup>-/-</sup> mice (Figure 1B), and bone volume was decreased in newborn *Maf*<sup>-/-</sup> mice (Figure 1C, Table 1, and Supplemental Figure 3). The formation of alkaline phosphatase-positive (ALP-positive) cells on an osteogenic front was markedly impaired in the calvaria of newborn *Maf*<sup>-/-</sup> mice (Figure 1D). In situ hybridization analysis revealed the expression of osteoblast genes, such as *Bglap1* (encoding osteocalcin), but not of *Runx2* was much lower in the embryos of *Maf*<sup>-/-</sup> mice than WT mice (Figure 1E and Supplemental Figure 4, A and B), although the proliferating or apoptotic osteoblast numbers were not different (Supplemental Figure 4C). Since the osteoclast number was decreased in *Maf*<sup>-/-</sup> mice, possibly in a cell-autonomous manner (Supplemental Figure 5), it is unlikely that abnormal osteoclastic bone resorption contributes to the low bone mass phenotype in *Maf*<sup>-/-</sup> mice. When a neomycin-resistance gene cassette was inserted into the *Maf* locus, chondrocyte development was reported to be affected in the mutant mice, but the mice were not perinatally lethal (18). In the current study, in which the coding sequence of *Maf* was entirely replaced by the *LacZ* cassette, the mice were perinatally lethal and exhibited more severe chondrocyte abnormalities (Supplemental Figure 6). It is difficult to rule out the possibility that a defect in chondrocytes contributes to a skeletal phenotype in long bone, but *Maf*<sup>-/-</sup> mice exhibited a defective bone formation in flat bones, like the calvaria (Figure 1B), which are not formed by endochondral bone formation, suggesting a role of *Maf* in osteoblasts. To analyze a cell-autonomous defect in osteoblasts further, osteoblast differentiation was evaluated in an in vitro culture system of osteoblast precursor cells derived from the calvaria of newborn *Maf*<sup>-/-</sup> mice. ALP activity and bone nodule formation were markedly suppressed in *Maf*<sup>-/-</sup> cells (Figure 2A), but neither the proliferation nor apoptosis was affected (Figure 2B). These results collectively indicate that a complete lack of *Maf* led to an osteopenic phenotype, due to impaired osteoblast differentiation and bone formation.

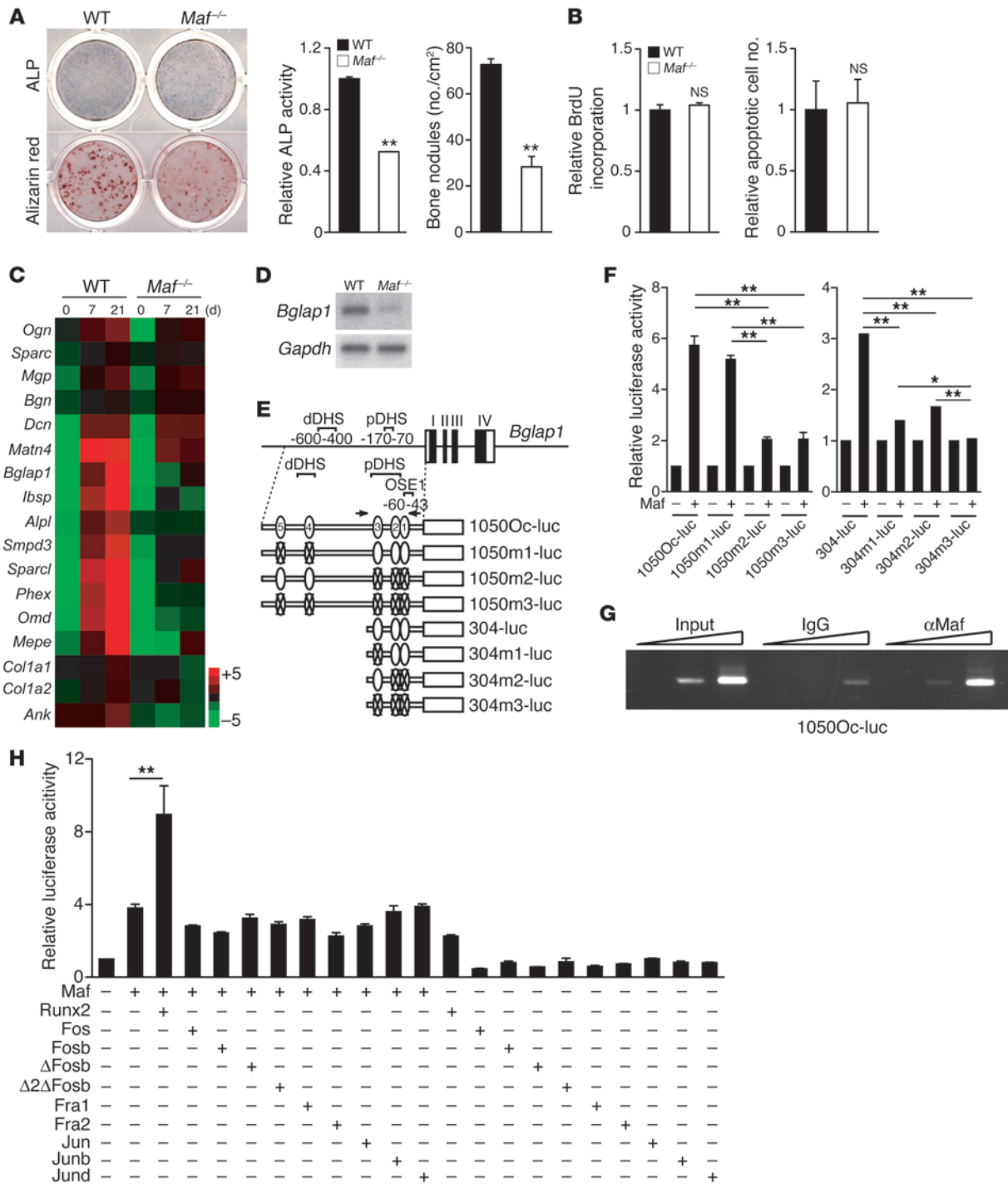
*Maf* regulates osteoblast differentiation in cooperation with *Runx2*. The expression of various osteoblast-specific genes, including *Bglap1*, was severely suppressed in *Maf*<sup>-/-</sup> cells (Figure 2, C and D), but *Runx2*, a well-known transcriptional regulator of *Bglap1* (21, 22), was normally expressed in *Maf*<sup>-/-</sup> mice (Supplemental Figure 4B). It is notable that *Maf* expression was not decreased in *Runx2*<sup>-/-</sup> calvarial osteoblasts (Supplemental Figure 7). These results prompted us to investigate whether *Maf* directly regulates the *Bglap1* promoter. As expected, 5 *Maf* recognition element-like (MARE-like) sequences were contained in the 1,050-base *Bglap1* promoter region (Figure 2E). A reporter gene assay indicated that *Maf* activates the *Bglap1* promoter mainly through a region containing 3 proximal MARE-like sequences (MARE1–MARE3), which was included in

the proximal DNase hypersensitive site (23) and partially overlapped with osteoblast-specific element 1 (OSE1) (22) (Figure 2F). ChIP experiments showed that *Maf* is recruited to the region containing MARE1–MARE3 in primary osteoblasts (Figure 2G), suggesting that *Maf* directly regulates the *Bglap1* promoter.

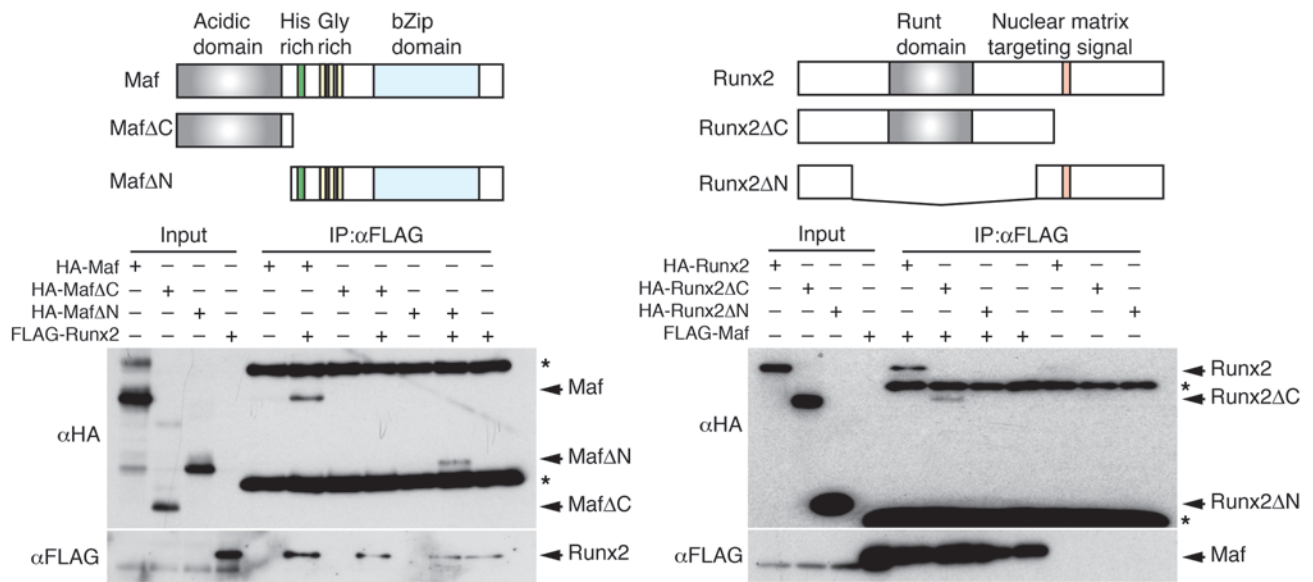
To gain insight into the transcriptional partners of *Maf*, we analyzed the *Maf* transcriptional network using a systems biology approach, based on protein-protein interaction databases and our own GeneChip analysis. Fos, Jun, Atf4, Nfat, and *Runx2* were included among the transcription factors predicted to interact with *Maf* (Supplemental Figure 8). The function of these candidate partners was examined in the *Maf*-mediated activation of the *Bglap1* promoter, which was found to be exclusively enhanced by the addition of *Runx2* (Figure 2H and data not shown). Consistent with this, the transcriptional activity of *Maf* on the *Bglap1* promoter was markedly decreased in *Runx2*<sup>-/-</sup> cells (Supplemental Figure 9). *Maf* bound to *Runx2* in an immunoprecipitation assay (Figure 3 and Supplemental Figure 10), and immunohistochemical analysis showed that *Maf* was colocalized with *Runx2* in calvarial osteoblasts (Supplemental Figure 11). Thus, these results suggest that *Maf* controls osteoblast differentiation by regulating osteoblastic gene expression mainly in cooperation with *Runx2*.

*Maf* suppresses adipogenesis by the downregulation of *Pparg*. We further characterized the *Maf*<sup>-/-</sup> calvarial cells using gene set enrichment analysis (GSEA), which revealed adipocyte-related genes to be highly enriched in *Maf*<sup>-/-</sup> cells (Supplemental Figure 12). Indeed, GeneChip data showed that the expression of adipocyte genes was upregulated in *Maf*<sup>-/-</sup> calvarial cells, even under the conditions optimized for osteoblast differentiation (Figure 4A). *Maf*<sup>-/-</sup> cells differentiated into oil red O-positive adipocytes more efficiently than WT cells (Figure 4B). Real-time RT-PCR analysis confirmed the expression of *Pparg*, the key transcription factor for adipogenesis, as well as that of *Fabp4*, *Slc2a4*, *Lpl*, *Acc1*, and *Cd36*, downstream effectors of *Pparγ* (24–26), to be markedly elevated in *Maf*<sup>-/-</sup> cells (Figure 4C and Supplemental Figure 13). To further investigate the role of *Maf* in osteoblast and adipocyte differentiation, we ectopically expressed *Maf* in C3H10T1/2 cells, a stromal cell line with a capacity to differentiate into both osteoblasts and adipocytes, and found that the introduction of *Maf* resulted in a severe blockade of adipocyte differentiation and an enhancement of osteoblast differentiation (Figure 4D and Supplemental Figure 14). Similar results were obtained using another stromal cell line, ST2, and BMSCs (Supplemental Figure 15, A–C). In addition, short hairpin RNA-mediated knockdown of *Maf* in ST2 cells resulted in a blockade of osteoblast differentiation and an acceleration of adipocyte differentiation (Supplemental Figure 15, D and E). Similar results were obtained using BMSCs (Supplemental Figure 15F). These results suggest that *Maf* promotes osteoblast differentiation and inhibits adipocyte differentiation in a cell-autonomous manner.

To understand the mechanism underlying the *Maf*-mediated inhibition of *Pparg* expression and adipogenesis, we examined the effect of *Maf* on the transcriptional activity of *Cebp*, the family members of which are involved in the regulation of *Pparg* (27, 28). Overexpression of *Maf* clearly suppressed the activation of the *Pparg* promoter by *Cebpα* and *Cebpδ* but not that by *Cebpβ* (Figure 4E and data not shown). Since the introduction of mutation(s) into MAREs in the *Pparg* promoter did not affect the inhibitory effect of *Maf* on *Cebpδ* activity, it is unlikely that *Maf* inhibited the *Pparg* promoter activity by directly binding to MAREs (Supplemental Figure 16, A and B). EMSA revealed that *Maf* did not affect the



**Figure 2** Regulation of osteoblast differentiation and *Bglap1* expression by Maf in cooperation with Runx2. (A) ALP and alizarin red staining of WT and *Maf*<sup>-/-</sup> calvarial cells. ALP activity and bone nodule formation were quantitated. (B) Proliferation and apoptosis of WT and *Maf*<sup>-/-</sup> calvarial cells. (C) mRNA expression of osteoblast-specific genes in WT and *Maf*<sup>-/-</sup> calvarial cells (GeneChip analysis). (D) *Bglap1* expression in WT and *Maf*<sup>-/-</sup> calvarial cells cultured with osteogenic medium for 7 days (RNA blot analysis). (E) Schematic of 5 MARE-like sequences (MARE1–MARE5) in the regulatory region of *Bglap1*, and *Bglap1*-luc variants harboring point mutation(s) in MARE-like sequences. pDHS and dDHS indicate proximal and distal DNase hypersensitive sites, respectively (23). Arrows indicate the primer set used for ChIP. Numbers within ovals represent corresponding MARE sequences. Ovals with “X”s indicate sequences without that respective MARE sequence. (F) Effect of Maf on the *Bglap1*-luc variants. (G) Recruitment of Maf to the *Bglap1* promoter region containing MARE1–MARE3. Calvarial cells cultured with osteogenic medium for 7 days were analyzed by ChIP. (H) Effect of Runx2 and AP-1 family members on Maf-mediated activation of 1050Oc-luc. \**P* < 0.05; \*\**P* < 0.01.

**Figure 3**

Physical interaction of Maf with Runx2. Maf and MafΔN, but not MafΔC, bound to Runx2. Runx2 and Runx2ΔC, but not Runx2ΔN, bound to Maf. Maf contains a transactivated domain (acidic domain), a histidine cluster (His rich), glycine stretches (Gly rich), and a basic leucine zipper domain (bZip domain). The asterisk indicates nonspecific bands.

DNA binding activity of Cebpδ, further supporting Maf-mediated inhibition of the *Pparg* promoter being independent of Maf binding to DNA (Supplemental Figure 16C). In addition, AP-1 family members and Runx2 did not affect Maf-mediated inhibition of the *Pparg* promoter (Supplemental Figure 16D). As it has been documented that Maf and Cebpδ commonly use CREB-binding protein gene (*Crebbp*) as their crucial transcriptional coactivator (29) (Supplemental Figure 8), we inferred that competition for the limited amount of *Crebbp* accounts for the inhibitory effect of Maf on the Cebpδ activity. As expected, the interaction of Cebpδ with *Crebbp* was suppressed by the overexpression of Maf (Figure 4F). Overexpression of *Crebbp* recovers the Maf-mediated inhibition of the effect of Cebpδ on the *Pparg* promoter (Figure 4E), lending support to the notion that Maf inhibits Cebpδ activity due to *Crebbp* squelching, although this may not be the sole mechanism underlying Maf inhibition of adipogenesis.

*Decreased Maf expression accelerates age-related osteoporosis and fatty bone marrow.* Although the perinatal lethality of *Maf*<sup>-/-</sup> mice renders it difficult to evaluate the development of fatty marrow with aging, the expression of *Pparg* in the bone marrow is much higher in perinatal *Maf*<sup>-/-</sup> mice than WT mice (Figure 5A), suggesting that the adipogenesis is enhanced in vivo in the case of *Maf* deficiency. Haploinsufficiency of *Maf* did not affect bone formation in embryos or neonatal mice (Figure 1B and Supplemental Figure 17). At the age of 22 weeks, however, histological analysis revealed that the bone marrow was filled with adipocytes characterized by fat vacuoles, and the bone volume was reduced in the *Maf*<sup>-/-</sup> mice (Figure 5, B and C, and Table 2). In contrast, no abnormalities in cartilage were found in the adult or neonatal *Maf*<sup>-/-</sup> mice (Supplemental Figures 6 and 18). The accelerated fatty marrow formation was accompanied by a decrease in osteoblast number and bone formation (Figure 5D), while osteoclastic bone resorption was not affected in the *Maf*<sup>-/-</sup> mice, with the serum calcium and phosphate levels being normally maintained (Supplemental Figures 19–21).

Thus, haploinsufficiency of *Maf* results in enhanced adipogenesis and decreased osteogenesis in vivo, which was obvious at an advanced age, suggesting that the decreasing level of *Maf* with age contributes to the age-related switch in mesenchymal cell differentiation into adipocytes rather than osteoblasts.

To determine whether forced expression of Maf in mesenchymal cells would rescue an aging phenotype of *Maf*<sup>-/-</sup> mice, we overexpressed Maf in calvarial cells by retroviral transfer and transplanted them into the femurs of aged mice (Supplemental Figure 22). *Maf*<sup>-/-</sup> mice transplanted with Maf-transduced calvarial cells had a higher trabecular bone mass (but not cortical bone mass) and a decreased number of intramedullary adipocytes compared with those transplanted with mock-infected calvarial cells (Figure 6A and Table 3). We observed similar results when we transplanted Maf-transduced calvarial cells into aged WT mice (Supplemental Figure 22D). These results indicate that overexpression of Maf resulted in effective restoration of both an accelerated aging phenotype in *Maf*<sup>-/-</sup> mice and age-related changes in WT mice.

*ROS regulation of Maf expression through Trp53.* How is *Maf* expression regulated during aging? Since it has been reported that age-related bone loss is related to an increased expression of the Wnt inhibitor secreted frizzled-related protein 4 (30) or a decreased production of soluble factors, such as IGF1, TGFβ1, IL-11, and bone morphogenetic protein 2 (6, 14, 15), we evaluated the effect of these factors as well as the effect of ROS on *Maf* expression. Although none of the soluble factors increased *Maf* expression in osteoblast precursor cells (Supplemental Figure 23), treatment with the hydrogen peroxide led to a marked decrease in *Maf* expression, which was restored by the addition of the antioxidant *N*-acetylcysteine (Figure 6B). These results prompted us to investigate whether administration of *N*-acetylcysteine rescue the bone phenotype of *Maf*<sup>-/-</sup> mice. As expected, administration of *N*-acetylcysteine led to an increased bone mass and decreased intramedullary fat in *Maf*<sup>-/-</sup> mice (Figure 6, C and D).

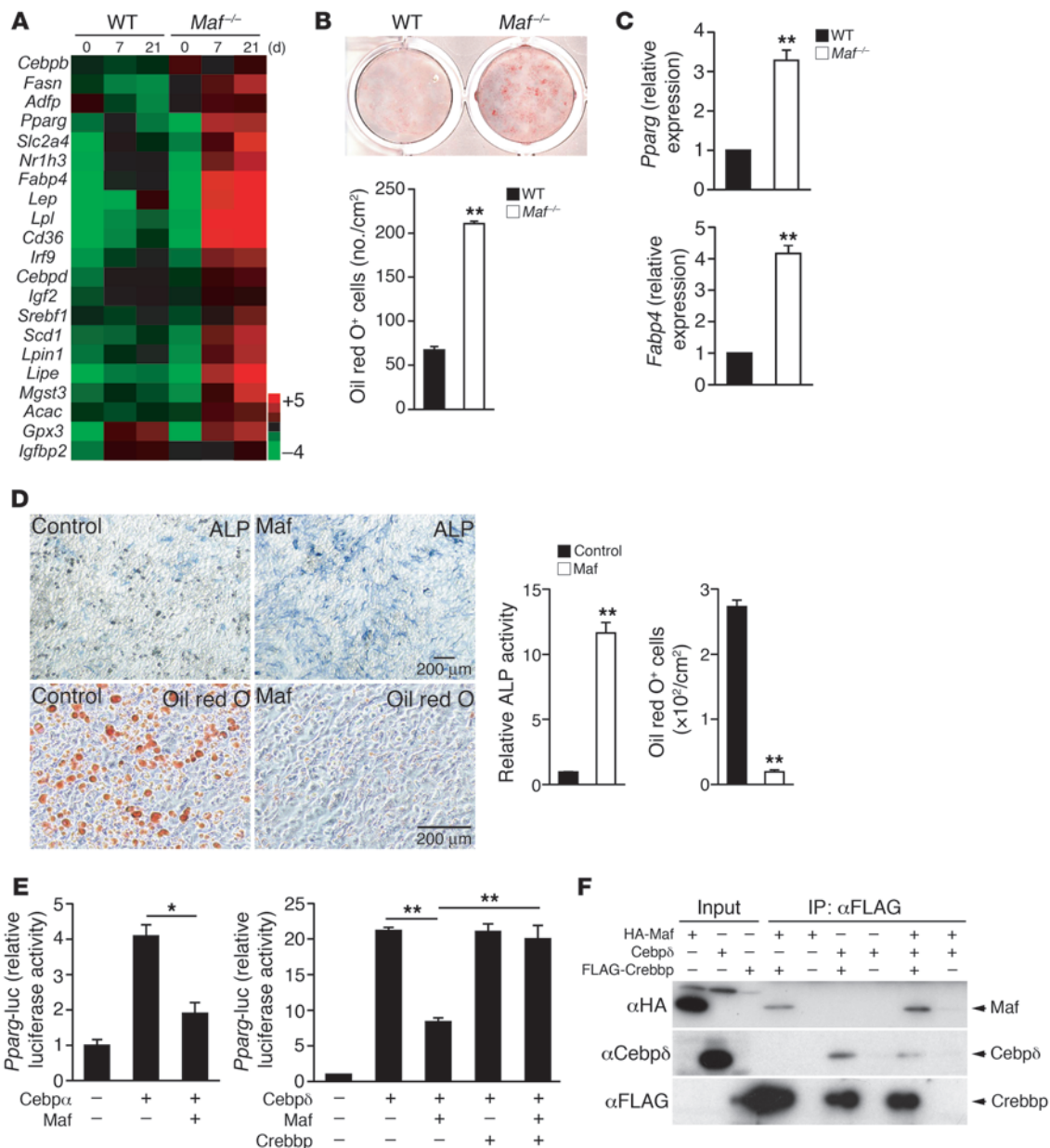


**Figure 4** Maf inhibition of adipocyte differentiation by suppressing Cebpb<sup>δ</sup>/α-mediated induction of *Pparg*. (A) mRNA expression of adipocyte-specific genes in WT and *Maf*<sup>-/-</sup> calvarial cells cultured with osteogenic medium (GeneChip analysis). (B) Adipocyte formation in WT and *Maf*<sup>-/-</sup> calvarial cells cultured with osteogenic medium (oil red O staining). (C) Expression of *Pparg* and *Fabp4* in WT and *Maf*<sup>-/-</sup> calvarial cells cultured with osteogenic medium (real-time RT-PCR analysis). (D) Effect of Maf overexpression on adipocyte and osteoblast differentiation of C3H10T1/2 cells. Scale bar: 200 μm. (E) Effect of Crebbp overexpression on Maf-mediated inhibition of Cebpb<sup>δ</sup> activation of the *Pparg* promoter. (F) Inhibition of interaction between Cebpb<sup>δ</sup> and Crebbp by Maf. \**P* < 0.05; \*\**P* < 0.01.

Furthermore, to gain mechanistic insight into the downregulation of *Maf* by ROS, we focused on the regulation of *Maf* by Trp53, which is reported to be induced by ROS and involved in aging (1, 2, 31, 32). Indeed, the *Maf* promoter contains multiple Trp53 binding sites and overexpression of Trp53 markedly inhibited the activity of the *Maf* promoter (Supplemental Figure 24). In addition, the downregulation of *Maf* by ROS was markedly attenuated in *Trp53*<sup>-/-</sup> osteoblasts (Figure 6B). Although NF-κB is involved in aging (33) and activated by ROS, *Maf* expression was not restored by an NF-κB inhibitor

(Supplemental Figure 25). These results suggest that the oxidative stress that accumulates with aging mediates, at least in part, the age-related decrease in *Maf* expression through Trp53.

### Discussion

The molecular basis for age-related changes in higher organisms is poorly understood, particularly in the skeletal system. Although many factors have been suggested to regulate the bifurcation of osteoblasts and adipocytes, the function of a few factors has been

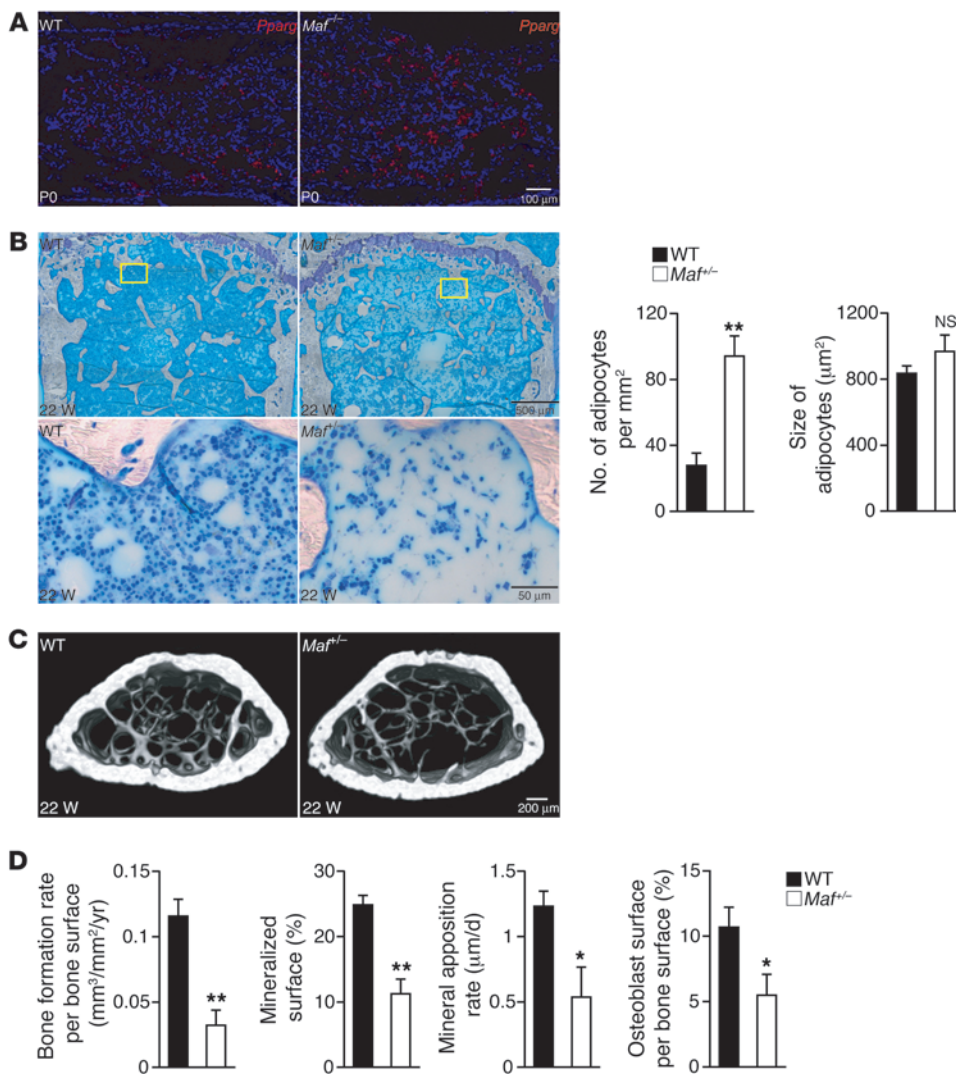


**Figure 5**

Increased adipogenesis in the *Maf* deficiency. (A) Expression of *Pparg* in the tibia of WT and *Maf*<sup>+/-</sup> littermates (in situ hybridization). Scale bar: 100 μm. (B) Histological analysis of the bone marrow of 22-week-old WT and *Maf*<sup>+/-</sup> female mice (femur, toluidine blue staining). Yellow boxed regions in the top panels are shown at higher magnification in the bottom panels. Note that *Maf*<sup>+/-</sup> bone marrow is filled with adipocytes. The number, but not the size, of adipocytes was significantly increased (*n* = 6). Scale bar: 500 μm (top row); 50 μm (bottom row). (C) Three-dimensional micro-computed tomography images of the femurs of 22-week-old WT and *Maf*<sup>+/-</sup> mice. Scale bar: 200 μm. (D) Parameters of osteoblastic bone formation in the bone morphometric analysis (*n* = 6; 22–26 weeks old). \**P* < 0.05; \*\**P* < 0.01.

demonstrated by genetic loss-of-function studies (7), and how the expression level of these factors changes in aging is not well known. A combination of a genome-wide screening and mouse genetic studies led us to identify the expression level of *Maf* to be both under the influence of aging and a determinant of mesenchymal cell differentiation into osteoblasts and adipocytes (Figure 6E).

*Maf* promotes osteoblast differentiation by regulating osteoblast genes, including *Bglap1*, in cooperation with Runx2. We propose that *Maf* functions as a modulator of bone formation by regulating the activity of crucial determinants like Runx2. Even in aged mice, bone marrow cells expressed a normal level of Runx2 (based on the screening shown in Figure 1A and Supplemental Table 1), but a low level of *Maf* expression resulted in a decrease in Runx2-mediated transcriptional activity. Therefore, *Maf* is a potential candidate to help explain the gradual and moderate decrease in bone formation observed in age-related osteoporosis. We also demonstrated that *Maf* inhibited adipocyte differentiation through the downregulation of *Pparg* expression, thus indicating that *Maf* regulates the bifurcation of the mesenchymal cell lineage into osteoblasts and adipocytes. It is interesting to note that the *MAF* locus was recently identified as one of the risk loci for obesity (34).

Using genetically modified mice, AP-1 superfamily members Fra1, Junb, and ΔFosb were shown to regulate bone formation (35–37), but ΔFosb was the only member that also regulates adipogenesis (19). However, since the adipogenic function of ΔFosb depends on a non-cell-autonomous mechanism (38), *Maf* is the only AP-1 superfamily member that has a cell-autonomous role in the regulation of both osteoblast and adipocyte differentiation. Interestingly, *Maf* also regulated osteoclastogenesis in a cell-autonomous manner, possibly by modulating NFAT activity (Sup-

**Table 2**

Skeletal development of 22-week-old *Maf*<sup>+/-</sup> mice

	WT	<i>Maf</i> <sup>+/-</sup>
BV/TV (%)	4.43 ± 0.15	3.17 ± 0.54 <sup>A</sup>
Tb.N (mm <sup>-1</sup> )	1.90 ± 0.02	1.54 ± 0.14 <sup>A</sup>
Tb.Sp (μm)	503.82 ± 5.69	623.86 ± 51.19 <sup>A</sup>
Tb.Th (μm)	23.35 ± 0.59	20.98 ± 0.60 <sup>A</sup>

Microcomputed tomography analysis of the femurs of 22-week-old WT and *Maf*<sup>+/-</sup> mice. <sup>A</sup>*P* < 0.05.

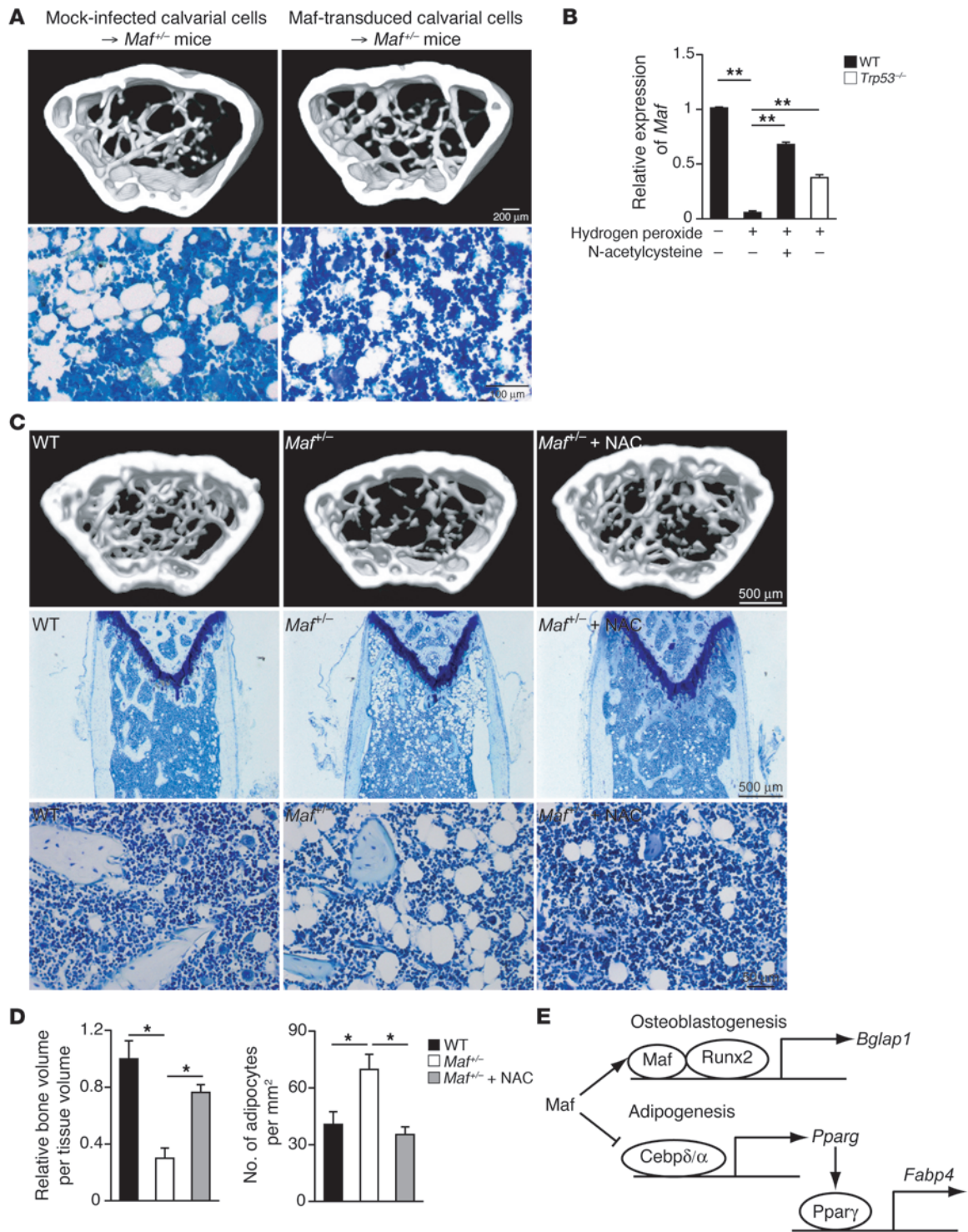


**Figure 6**

Aging and *Maf*-mediated regulation of osteoblastogenesis and adipogenesis. **(A)** Effect of *Maf* overexpression in mesenchymal cells on an aging phenotype of *Maf*<sup>+/+</sup> mice. Three-dimensional microcomputed tomography images and histological analysis of the bone marrow (toluidine blue staining) of *Maf*<sup>+/+</sup> mice transplanted with *Maf*-transduced or mock-infected calvarial cells. Scale bar: 200 μm (top row); 100 μm (bottom row). **(B)** Effect of hydrogen peroxide on *Maf* expression in WT and *Trp53*<sup>-/-</sup> calvarial osteoblasts (real-time RT-PCR analysis). **(C)** Effect of *N*-acetylcysteine (NAC) administration on an aging phenotype of *Maf*<sup>+/+</sup> mice. Three-dimensional microcomputed tomography images (top row) and histology of the bone marrow (toluidine blue staining, middle and bottom rows) of mice (*n* = 4). Images in the middle row are shown at higher magnification in the bottom row. Scale bar: 500 μm (top and middle rows); 50 μm (bottom row). **(D)** Microcomputed tomography and histological analysis of WT and *Maf*<sup>+/+</sup> mice. **(E)** A model of *Maf*-mediated reciprocal regulation of osteoblast and adipocyte differentiation. \**P* < 0.05; \*\**P* < 0.01.



**Table 3**  
Skeletal development and adipogenesis in *Maf*<sup>+/-</sup> mice transplanted with *Maf*-transduced and mock-infected calvarial cells

	Mock-infected calvarial cells	<i>Maf</i> -transduced calvarial cells
BV/TV (%)	4.95 ± 0.77	6.81 ± 0.57 <sup>A</sup>
CV/TV (%)	35.06 ± 0.43	35.09 ± 0.71
Adipocytes (mm <sup>-2</sup> )	97.1 ± 6.6	62.8 ± 6.7 <sup>B</sup>

Effect of *Maf* overexpression in mesenchymal cells on an aging phenotype of *Maf*<sup>+/-</sup> mice (*n* = 4). CV/TV, cortical bone volume/total volume. <sup>A</sup>*P* < 0.05. <sup>B</sup>*P* < 0.01.

plemental Figure 5, C and E), suggesting that *Maf* plays a distinct role in each skeletal cell type.

Since *Pparγ* inhibits the expression of *Maf* (39), a small reduction in *Maf* expression would form a vicious cycle: an increasing expression of *Pparγ* further inhibits *Maf* expression, leading to a severe reduction in *Maf*. Antidiabetic drugs — such as TZDs, which activate *Pparγ* — are known to reduce bone mass and increase fracture risk (12). Interestingly, treatment with rosiglitazone led to decreased *Maf* expression (data not shown). This is possibly because *Pparγ* agonists accelerate this vicious cycle through suppression of *Maf* expression.

Mathematical modeling of gene expression is helpful for understanding how the gradual reduction of *Maf* expression leads to a dramatic change in cell differentiation. Based on this simulation, if the expression of *Maf* decreased by more than 60% of the maximum level, the adipogenic genes became preferentially expressed (Supplemental Figure 26 and Supplemental Methods). Reduction of *Maf* gene expression in neonatal *Maf*<sup>+/-</sup> mice was not sufficient for activation of this switch, as we observed no obvious bone phenotype in neonatal *Maf*<sup>+/-</sup> mice (Figure 1B and Supplemental Figure 17). As the level of *Maf* gradually decreased with age, they exhibited an osteopenic phenotype with fatty marrow.

Currently, there are few drugs available in the clinic that effectively increase bone formation. The modulation of *Maf* expression appears to hold considerable promise as what we believe to be a novel antiaging therapeutic target in the skeletal system.

## Methods

**Mice.** *Maf*<sup>+/-</sup> mice were previously generated and described elsewhere (16). *Maf*<sup>+/-</sup> mice were backcrossed into C57BL/6 mice for more than 9 generations, unless otherwise described. All mice were born and maintained under specific pathogen-free conditions. All animal experiments were performed with the approval of the Animal Study Committee of Tokyo Medical and Dental University and conformed to relevant guidelines and laws.

**Microcomputed tomography analysis.** CT scanning was performed using a ScanXmate-A100S Scanner (Comscantechno). Three-dimensional microstructural image data were reconstructed and structural indices were calculated using TRI/3D-BON software (RATOC). Bone mineral density (BMD) was calculated using TRI/3D-BON-BMD-PNTM software (RATOC). Bone morphometric and BMD analyses were performed at a region 0.8–1.8 mm above the distal growth plate of the femur in adult mice and using the full-length femur in postnatal mice, unless otherwise described.

**In situ hybridization and immunohistochemical analysis.** Embryos and bones were fixed in 4% paraformaldehyde, embedded in paraffin, and sectioned (5 μm). In situ hybridization was performed using <sup>35</sup>S-labeled *Bglap1*, *Runx2*, and *Col1a1* probes as described previously (40). The *Pparγ* probe

is a 521-bp fragment of the *Pparγ* coding region. Immunohistochemical analysis was performed using a standard avidin-biotin peroxidase method (Vector Laboratories), according to the manufacturer's protocols. Paraffin-embedded sections were dewaxed, rehydrated, and subjected to an antigen retrieval procedure. The sections were then blocked with 5% lamb serum and incubated with the antibody. The antibodies are listed in Supplemental Table 2. For the proliferation assay, pregnant mice were injected with BrdU 1 hour before sacrifice. We detected mitotic cells using the BrdU Staining Kit (Zymed) and detected apoptotic cells by TUNEL staining with the ApoAlert DNA Fragmentation Kit (Clontech).

**Cell cultures.** For in vitro osteoblast and adipocyte differentiation, cells derived from bone marrow or calvaria were cultured with osteogenic medium (50 μM ascorbic acid, 10 nM dexamethasone, and 10 mM β-glycerophosphate) or adipogenic medium (0.5 mM 3-isobutyl-1-methylxanthine, 5 μg/ml insulin, and 1 μM dexamethasone), as described previously (20, 41). ALP assay (7 days of culture), alizarin red staining (21 days of culture), and oil red O staining (10 days of culture) were performed as previously described (20, 41). We determined the rate of cell proliferation using the Cell Proliferation ELISA kit (Roche) and detected apoptotic cells by TUNEL staining with the MEBSTATIN Apoptosis Kit Direct (MBL). The method for in vitro osteoclast differentiation was described previously (42–44). Briefly, bone marrow-, fetal liver-, or spleen-derived cells, cultured with 10 ng/ml M-CSF (R&D Systems) for 2 days, were used as osteoclast precursor cells, which were further cultured with 50 ng/ml RANKL (Peprotech) in the presence of 10 ng/ml M-CSF for 3 days. In the coculture system used to generate osteoclasts, bone marrow cells were cultured with calvarial cells in the presence of 1 nM 1,25-dihydroxyvitamin D<sub>3</sub> (Wako) and 1 μM prostaglandin E<sub>2</sub> (Cayman Chemical) for 7 days.

To obtain the stable transformants constitutively expressing *Maf*, the retroviral vectors pMX-HA-*Maf*-IRES-Puro and pMX-IRES-Puro, as the control, were introduced into C3H10T1/2 and ST2 clonal cells, and the stable transformants were selected with puromycin. To establish the stable transformants expressing shRNAs targeting *Maf*, the retroviral vectors pSIREN-sh*Maf* and pSIREN-shControl were introduced into ST2 clonal cells, and stable transformants were selected with puromycin. For osteoblast and adipocyte differentiation, transformants were cultured under an osteogenic condition (50 μM ascorbic acid, 10 nM dexamethasone, 10 mM β-glycerophosphate, and 100 ng/ml BMP2) and adipogenic condition (0.26 mM 3-isobutyl-1-methylxanthine, 85 nM insulin, and 0.5 μM dexamethasone), respectively.

**Transplantation of *Maf*-transduced calvarial cells.** The transplantation experiment was performed as described previously (45) with minor modifications. Briefly, we used 32-week-old WT and *Maf*<sup>+/-</sup> mice as recipients and newborn *Maf*<sup>+/-</sup> mice as donors. The mice were obtained from an intercross between *Maf*<sup>+/-</sup> mice, which are backcrossed into C57BL/6 mice for more than 9 generations. The mice were anesthetized by an injection of somnopenyl into the peritoneal cavity, and the proximal femur was gently drilled with a diamond-coated burr. Cells were obtained from calvaria derived from newborn *Maf*<sup>+/-</sup> mice and transduced with a retroviral vector (pMX-HA-*Maf*-IRES-GFP or pMX-IRES-GFP). The *Maf*-transduced or mock-infected calvarial cells were directly injected into the bone marrow cavity through the hole in the femur using a 28-gauge needle (approximately 1 × 10<sup>5</sup> cells per femur). The needle was inserted almost to the distal metaphysis. After transplantation, the drilled hole was filled with bone cement (Fuji Lute, GC). The mice were analyzed 1 month after transplantation. Microcomputed tomography analysis and measurement of fat marrow were performed within 1 mm above the distal growth plate of the femur.

**Administration of *N*-acetylcysteine.** *Maf*<sup>+/-</sup> mice were backcrossed into C57BL/6 mice for more than 3 generations. Mice were supplied drinking water containing 2 mg/ml *N*-acetylcysteine ad libitum for 14 weeks. At 22 weeks of age, mice were sacrificed and analyzed.



**RNA blot and real-time RT-PCR analyses.** Total RNA was extracted with ISOGEN (Wako) or the RNeasy Lipid Tissue Mini Kit (Qiagen). Total RNA was blotted and hybridized with [ $\alpha$ - $^{32}$ P]dCTP-labeled probes for *Maf*, *Bglap1*, and *Gapdh*, as described previously (39, 41). Real-time RT-PCR was performed with a LightCycler (Roche) using SYBR Green (Toyobo) as described previously (44). The primer sequences are listed in Supplemental Table 3.

**GeneChip analysis.** GeneChip analysis, clustering analysis, and GSEA were performed as described previously (42, 46, 47). Calvarial cells cultured with osteogenic medium for 0, 7, and 21 days were analyzed. BMSCs derived from 8- and 32-week-old mice were isolated as described previously (48) with minor modifications. Briefly, bone marrow cells from each of the mice were isolated by flushing the femurs and tibiae with  $\alpha$ -MEM with 10% FBS, and these cells were plated on plastic dishes. After 3 days, adherent cells were used. BMSCs contain a precursor of osteoblasts and adipocytes (data not shown) (49). The total RNAs extracted from these cells were used for cDNA synthesis by reverse transcription, followed by synthesis of biotinylated cRNA through in vitro transcription. After cRNA fragmentation, hybridization with the Mouse Genome 430 2.0 Array (Affymetrix) was performed as described previously (42). The main part of the data set was deposited and can be obtained from the Genome Network Platform (<http://genomeweb.nig.ac.jp/>).

**ChIP assay.** After calvarial cells were cultured with osteogenic medium for 7 days, ChIP assay was performed using the ChIP Assay Kit (Upstate) with minor modification. The antibodies used are listed in Supplemental Table 2. The primer sequences are listed in Supplemental Table 3.

**Retroviral gene transfer.** Retroviral vectors pMX-HA-Maf-IRES-GFP and pMX-HA-Maf-IRES-Puro were constructed by inserting DNA fragments encoding HA and Maf into pMX-IRES-GFP and pMX-IRES-Puro (50). Retroviral vectors pSIREN-shMaf and pSIREN-shControl were constructed by inserting annealed oligonucleotide into RNAi-Ready pSIREN-RetroQ (BD Biosciences). The oligonucleotide sequences are listed in Supplemental Table 3. Retroviral packaging was performed by transfecting the plasmids into Plat-E or Plat-A cells using FuGENE6 as described previously (50).

**Reporter gene assay.** The reporter plasmids, *Bglap1*-luc variants, were constructed from 1050Oc-luc (41), and mutations in MARE-like sequences were introduced by PCR. A site-directed mutagenesis performed with sequential PCR steps was used to engineer the mutated MARE-like sequences. Two overlapping PCR fragments, each containing the MARE1-MARE5 mutation, were generated. The corresponding PCR fragments were used as templates for the second PCR step. The primer sequences are listed in Supplemental Table 3. *Maf*-luc was constructed by subcloning a 2-kb fragment of the 5' flanking region of the *Maf* gene into the pGL3-basic vector (Promega). Luciferase assay was performed in NIH3T3 cells or mouse embryonic fibroblasts (MEFs) established from WT and *Runx2*<sup>-/-</sup> E14 embryos (51). *Pparg*-luc was constructed by subcloning a 2.2-kb fragment of the 5' flanking region of the *Pparg* gene (52) into the pGL3-basic vector, and mutations in MAREs were introduced by PCR. The primer sequences are listed in Supplemental Table 3. Luciferase assay was performed in 3T3-L1 cells. The expression plasmids of Maf, Runx2, Fos, Fosb, Fosl1, Fosl2, Jun, Junb, Jund, Cebp $\alpha$ , Cebp $\beta$ , Cebp $\delta$ , Crebbp, p50, p65, and Tp53 have been described elsewhere (16, 41, 42, 53–58). The expression plasmids of  $\Delta$ Fosb and  $\Delta$ 2 $\Delta$ Fosb were constructed from full-length Fosb cDNA using PCR. The reporter plasmids (p*Acp5*-luc, ref. 42, and p*Nfatc1*-luc, ref. 43) were described previously. MEFs and NIH3T3 and 3T3-L1 cells were transfected using Lipofectamine plus reagents (Invitrogen). After 30–36 hours, dual luciferase assay was performed according to the manufacturer's protocols (Promega).

**Immunoblot and immunoprecipitation analyses.** Immunoblot and immunoprecipitation analyses were performed as previously described (59). The

antibodies used are listed in Supplemental Table 2. For analyzing the interaction between Maf and Runx2, HA-tagged Maf, HA-tagged N-terminal region of Maf (HA-tagged Maf $\Delta$ C), HA-tagged C-terminal region of Maf (HA-tagged Maf $\Delta$ N), HA-tagged Runx2, HA-tagged Runx2 $\Delta$ N, HA-tagged Runx2 $\Delta$ C, FLAG-tagged Maf, and FLAG-tagged Runx2 proteins were produced by the in vitro transcription/translation system (Promega). These proteins were mixed in a binding buffer and incubated with anti-FLAG antibody-conjugated agarose beads (Sigma-Aldrich). Recovered proteins were subjected to immunoblot analysis with anti-FLAG and anti-HA antibodies. For analyzing the interaction among Maf, Cebp $\delta$ , and Crebbp, HA-tagged Maf and Cebp $\delta$  proteins were produced by the in vitro transcription/translation system. FLAG-tagged Crebbp proteins were produced by transfecting FLAG-Crebbp expression plasmids into HEK293T cells using FuGENE6 (Roche). These proteins were mixed and incubated with anti-FLAG antibody-conjugated agarose beads. Recovered proteins were subjected to immunoblot analysis with anti-Cebp $\delta$ , anti-FLAG, and anti-HA antibodies.

**Treatment of *Trp53*<sup>-/-</sup> osteoblasts with hydrogen peroxide.** Osteoblasts were isolated from the calvaria of newborn mice deficient in *Trp53* (accession no., CDB0001K; <http://www.cdb.riken.jp/arg/mutant%20mice%20list.html>) (60) and treated with 600  $\mu$ M hydrogen peroxide. Five days after the treatment, mRNAs were extracted and subjected to real-time PCR analysis.

**EMSA.** EMSA was performed as previously described (59). Maf and Cebp $\delta$  proteins were produced by the in vitro transcription/translation system. The CCAAT probe for binding of Cebp $\delta$  and the MARE probe for binding of Maf were generated by annealing synthetic oligonucleotides. The oligonucleotide sequences are listed in Supplemental Table 3. Antibodies against Maf and Cebp $\delta$  were used for supershift analysis.

**ELISA.** Soluble osteocalcin levels and TRAP activity in serum were detected using the mouse osteocalcin EIA kit (Biomedical Technologies Inc.) and mouse TRAP assay (SBA Sciences), respectively.

**Statistics.** Statistical analysis was performed using Student's *t* test for comparisons between 2 groups and analysis of variance with Bonferroni post-hoc test for comparisons among 3 or more groups, unless otherwise described. All data are expressed as mean  $\pm$  SEM.

## Acknowledgments

We thank H.R. Ueda, M. Asagiri, T. Ando, Y. Kunisawa, T. Honda, Y. Suzuki, T. Kudo, A. Izumi, A. Suematsu, and A. Hirota for discussion and assistance. This work was supported in part by a grant for ERATO from the Takayanagi Osteonetwork Project from the Japan Science and Technology Agency; Grant-in-Aids for Creative Scientific Research and Young Scientist (A and Startup) from the Japan Society for the Promotion of Science (JSPS); Grant-in-Aid for Challenging Exploratory Research JSPS; grants for the Genome Network Project and Global Center of Excellence Program from the Ministry of Education, Culture, Sports, Science and Technology of Japan; and grants from Tokyo Biochemical Research Foundation, Life Science Foundation of Japan, Yokoyama Foundation for Clinical Pharmacology, and Takeda Science Foundation.

Received for publication February 1, 2010, and accepted in revised form July 14, 2010.

Address correspondence to: Hiroshi Takayanagi, Department of Cell Signaling, Graduate School of Medical and Dental Sciences, Tokyo Medical and Dental University, Yushima 1-5-45, Bunkyo-ku, Tokyo 113-8549, Japan. Phone: 81.3.5803.5471; Fax: 81.3.5803.0192; E-mail: taka.csi@tmd.ac.jp.



- Collado M, Blasco MA, Serrano M. Cellular senescence in cancer and aging. *Cell*. 2007;130(2):223–233.
- Chen JH, Hales CN, Ozanne SE. DNA damage, cellular senescence and organismal ageing: causal or correlative? *Nucleic Acids Res*. 2007;35(22):7417–7428.
- Uccelli A, Moretta L, Pistonia V. Mesenchymal stem cells in health and disease. *Nat Rev Immunol*. 2008;8(9):726–736.
- Engler AJ, Sen S, Sweeney HL, Discher DE. Matrix elasticity directs stem cell lineage specification. *Cell*. 2006;126(4):677–689.
- Meunier P, Aaron J, Edouard C, Vignon G. Osteoporosis and the replacement of cell populations of the marrow by adipose tissue. A quantitative study of 84 iliac bone biopsies. *Clin Orthop Relat Res*. 1971; 80:147–154.
- Manolagas SC. Birth and death of bone cells: basic regulatory mechanisms and implications for the pathogenesis and treatment of osteoporosis. *Endocr Rev*. 2000;21(2):115–137.
- Gimble JM, Zvonic S, Floyd ZE, Kassem M, Nuttall ME. Playing with bone and fat. *J Cell Biochem*. 2006;98(2):251–266.
- Belaïd-Choucair Z, et al. Human bone marrow adipocytes block granulopoiesis through neuropilin-1-induced granulocyte colony-stimulating factor inhibition. *Stem Cells*. 2008;26(6):1556–1564.
- Corre J, Planat-Benard V, Corberand JX, Penicaud L, Casteilla L, Laharrague P. Human bone marrow adipocytes support complete myeloid and lymphoid differentiation from human CD34 cells. *Br J Haematol*. 2004;127(3):344–347.
- Maurin AC, Chavassieux PM, Frappart L, Delmas PD, Serre CM, Meunier PJ. Influence of mature adipocytes on osteoblast proliferation in human primary cocultures. *Bone*. 2000;26(5):485–489.
- Naveiras O, Nardi V, Wenzel PL, Hauschka PV, Fahey F, Daley GQ. Bone-marrow adipocytes as negative regulators of the haematopoietic microenvironment. *Nature*. 2009;460(7252):259–263.
- McDonough AK, Rosenthal RS, Cao X, Saag KG. The effect of thiazolidinediones on BMD and osteoporosis. *Nat Clin Pract Endocrinol Metab*. 2008; 4(9):507–513.
- Seeman E, Delmas PD. Bone quality--the material and structural basis of bone strength and fragility. *N Engl J Med*. 2006;354(21):2250–2261.
- Lamberts SW, van den Beld AW, van der Lely AJ. The endocrinology of aging. *Science*. 1997; 278(5337):419–424.
- Lambert CJ. Growth hormone, insulin-like growth factors, and the senescent skeleton: Ponce de Leon's Fountain revisited? *J Cell Biochem*. 1994; 56(3):348–356.
- Kawauchi S, et al. Regulation of lens fiber cell differentiation by transcription factor c-Maf. *J Biol Chem*. 1999;274(27):19254–19260.
- Ho IC, Glimcher LH. Transcription: tantalizing times for T cells. *Cell*. 2002;109 suppl:S109–S120.
- MacLean HE, Kim JI, Glimcher MJ, Wang J, Kronenberg HM, Glimcher LH. Absence of transcription factor c-maf causes abnormal terminal differentiation of hypertrophic chondrocytes during endochondral bone development. *Dev Biol*. 2003;262(1):51–63.
- Sabatakos G, et al. Overexpression of DeltaFosB transcription factor(s) increases bone formation and inhibits adipogenesis. *Nat Med*. 2000;6(9):985–990.
- Hong JH, et al. TAZ, a transcriptional modulator of mesenchymal stem cell differentiation. *Science*. 2005;309(5737):1074–1078.
- Karsenty G, Wagner EF. Reaching a genetic and molecular understanding of skeletal development. *Dev Cell*. 2002;2(4):389–406.
- Yang X, et al. ATF4 is a substrate of RSK2 and an essential regulator of osteoblast biology; implication for Coffin-Lowry Syndrome. *Cell*. 2004; 117(3):387–398.
- Montecino M, Lian J, Stein G, Stein J. Changes in chromatin structure support constitutive and developmentally regulated transcription of the bone-specific osteocalcin gene in osteoblastic cells. *Biochemistry*. 1996;35(15):5093–5102.
- Lee CH, Olson P, Evans RM. Minireview: lipid metabolism, metabolic diseases, and peroxisome proliferator-activated receptors. *Endocrinology*. 2003; 144(6):2201–2207.
- Farmer SR. Transcriptional control of adipocyte formation. *Cell Metab*. 2006;4(4):263–273.
- Tontonoz P, Spiegelman BM. Fat and beyond: the diverse biology of PPARgamma. *Annu Rev Biochem*. 2008;77:289–312.
- Shi XM, Blair HC, Yang X, McDonald JM, Cao X. Tandem repeat of C/EBP binding sites mediates PPARgamma2 gene transcription in glucocorticoid-induced adipocyte differentiation. *J Cell Biochem*. 2000;76(3):518–527.
- Wu Z, et al. Cross-regulation of C/EBP alpha and PPAR gamma controls the transcriptional pathway of adipogenesis and insulin sensitivity. *Mol Cell*. 1999;3(2):151–158.
- Kovacs KA, Steinmann M, Magistretti PJ, Halfon O, Cardinaux JR. CCAAT/enhancer-binding protein family members recruit the coactivator CREB-binding protein and trigger its phosphorylation. *J Biol Chem*. 2003;278(38):36959–36965.
- Nakanishi R, et al. Secreted frizzled-related protein 4 is a negative regulator of peak BMD in SAMP6 mice. *J Bone Miner Res*. 2006;21(11):1713–1721.
- Almeida M, et al. Skeletal involution by age-associated oxidative stress and its acceleration by loss of sex steroids. *J Biol Chem*. 2007;282(37):27285–27297.
- Tyner SD, et al. p53 mutant mice that display early ageing-associated phenotypes. *Nature*. 2002; 415(6867):45–53.
- Adler AS, Sinha S, Kawahara TL, Zhang JY, Segal E, Chang HY. Motif module map reveals enforcement of aging by continual NF-kappaB activity. *Genes Dev*. 2007;21(24):3244–3257.
- Meyre D, et al. Genome-wide association study for early-onset and morbid adult obesity identifies three new risk loci in European populations. *Nat Genet*. 2009;41(2):157–159.
- Jochum W, et al. Increased bone formation and osteosclerosis in mice overexpressing the transcription factor Fra-1. *Nat Med*. 2000;6(9):980–984.
- Eferl R, et al. The Fos-related antigen Fra-1 is an activator of bone matrix formation. *EMBO J*. 2004; 23(14):2789–2799.
- Kenner L, et al. Mice lacking JunB are osteopenic due to cell-autonomous osteoblast and osteoclast defects. *J Cell Biol*. 2004;164(4):613–623.
- Rowe GC, Choi CS, Neff L, Horne WC, Shulman GI, Baron R. Increased energy expenditure and insulin sensitivity in the high bone mass DeltaFosB transgenic mice. *Endocrinology*. 2009;150(1):135–143.
- Serria MS, Ikeda H, Omoteyama K, Hirokawa J, Nishi S, Sakai M. Regulation and differential expression of the c-maf gene in differentiating cultured cells. *Biochem Biophys Res Commun*. 2003; 310(2):318–326.
- Takeda S, Bonnamy JP, Owen MJ, Ducy P, Karsenty G. Continuous expression of Cbfa1 in nonhypertrophic chondrocytes uncovers its ability to induce hypertrophic chondrocyte differentiation and partially rescues Cbfa1-deficient mice. *Genes Dev*. 2001; 15(4):467–481.
- Kim S, et al. Stat1 functions as a cytoplasmic attenuator of Runx2 in the transcriptional program of osteoblast differentiation. *Genes Dev*. 2003; 17(16):1979–1991.
- Takayanagi H, et al. Induction and activation of the transcription factor NFATc1 (NFAT2) integrate RANKL signaling in terminal differentiation of osteoclasts. *Dev Cell*. 2002;3(6):889–901.
- Asagiri M, et al. Autoamplification of NFATc1 expression determines its essential role in bone homeostasis. *J Exp Med*. 2005;202(9):1261–1269.
- Nishikawa K, et al. Blimp1-mediated repression of negative regulators is required for osteoclast differentiation. *Proc Natl Acad Sci U S A*. 2010; 107(7):3117–3122.
- Zhang XS, et al. Local ex vivo gene therapy with bone marrow stromal cells expressing human BMP4 promotes endosteal bone formation in mice. *J Gene Med*. 2004;6(1):4–15.
- Eisen MB, Spellman PT, Brown PO, Botstein D. Cluster analysis and display of genome-wide expression patterns. *Proc Natl Acad Sci U S A*. 1998; 95(25):14863–14868.
- Subramanian A, et al. Gene set enrichment analysis: a knowledge-based approach for interpreting genome-wide expression profiles. *Proc Natl Acad Sci U S A*. 2005;102(43):15545–15550.
- Xiao Y, Fu H, Prasadam I, Yang YC, Hollinger JO. Gene expression profiling of bone marrow stromal cells from juvenile, adult, aged and osteoporotic rats: with an emphasis on osteoporosis. *Bone*. 2007;40(3):700–715.
- Holmes C, Khan TS, Owen C, Ciliberti N, Grynblas MD, Stanford WL. Longitudinal analysis of mesenchymal progenitors and bone quality in the stem cell antigen-1-null osteoporotic mouse. *J Bone Miner Res*. 2007;22(9):1373–1386.
- Morita S, Kojima T, Kitamura T. Plat-E: an efficient and stable system for transient packaging of retroviruses. *Gene Ther*. 2000;7(12):1063–1066.
- Otto F, et al. Cbfa1, a candidate gene for cleidocranial dysplasia syndrome, is essential for osteoblast differentiation and bone development. *Cell*. 1997;89(5):765–771.
- Kudo M, Sugawara A, Uruno A, Takeuchi K, Ito S. Transcription suppression of peroxisome proliferator-activated receptor gamma2 gene expression by tumor necrosis factor alpha via an inhibition of CCAAT/enhancer-binding protein delta during the early stage of adipocyte differentiation. *Endocrinology*. 2004;145(11):4948–4956.
- Nishiyori A, et al. Determination of tissue specificity of the enhancer by combinatorial operation of tissue-enriched transcription factors. Both HNF-4 and C/EBP beta are required for liver-specific activity of the ornithine transcarbamylase enhancer. *J Biol Chem*. 1994;269(2):1323–1331.
- Matsuo K, Owens JM, Tonko M, Elliott C, Chambers TJ, Wagner EF. Fos1 is a transcriptional target of c-Fos during osteoclast differentiation. *Nat Genet*. 2000;24(2):184–187.
- Ohoka N, Yoshii S, Hattori T, Onozaki K, Hayashi H. TRB3, a novel ER stress-inducible gene, is induced via ATP4-CHOP pathway and is involved in cell death. *EMBO J*. 2005;24(6):1243–1255.
- Kawai J, et al. Functional annotation of a full-length mouse cDNA collection. *Nature*. 2001; 409(6821):685–690.
- Koga T, et al. NFAT and Osterix cooperatively regulate bone formation. *Nat Med*. 2005;11(8):880–885.
- Tanikawa J, et al. p53 suppresses the c-Myb-induced activation of heat shock transcription factor 3. *J Biol Chem*. 2000;275(20):15578–15585.
- Nishikawa K, et al. Self-association of Gata1 enhances transcriptional activity in vivo in zebra fish embryos. *Mol Cell Biol*. 2003;23(22):8295–8305.
- Tsukada T, et al. Enhanced proliferative potential in culture of cells from p53-deficient mice. *Oncogene*. 1993;8(12):3313–3322.